Thin Film Rheology and Tribology of Confined Polymer Melts: Contrasts with Bulk Properties

Gustavo Luengo, Franz-Josef Schmitt,† Robert Hill, and Jacob Israelachvili*

Department of Chemical Engineering and Materials Department, University of California, Santa Barbara, California 93106-5080

Received December 26, 1995; Revised Manuscript Received August 12, 1996[⊗]

ABSTRACT: A modified Surface Forces Apparatus was used for making rheological and tribological measurements of thin fluid films, and polybutadiene (PBD) of $M_w \approx 7000$ was studied in detail. At low shear rates, PBD exhibits bulklike properties in films thicker than about 200 nm. In thinner films (200−20 nm), the shear viscosity η_{eff} and moduli G' and G'' become quantitatively modified from those of the bulk. However, a sinusoidal input still produces a sinusoidal output, and a modified WLF representation remains applicable to such films. On entering the tribological regime (film thickness <30 nm) polybutadiene exhibits highly nonlinear behavior and yield points, indicative of phase transitions to "glassy" or "solidlike" states. Other features are (i) a shift of the slip plane, (ii) an additional normal force component, and (iii) the emergence of new scaling relationships for η_{eff}, G', G'', and the friction force F as a function of frequency, sliding speed, and other system parameters.

Introduction

There is currently much interest in understanding the structure and dynamics of fluid molecules in confined geometries, for example, during flow through narrow pores or in thin lubricating films between two shearing surfaces. Such systems have an obvious practical value, but they are also of great fundamental and theoretical interest because the properties of confined complex molecules, such as polymers, can be very different from their properties in the bulk.

In the simplest ideal case (Figure 1) of two planar surfaces of area S, separated at a distance D by a Newtonian fluid of shear viscosity η, the shear or "friction" force F during sliding at velocity V is given by the standard equation for Couette flow

$$F = \frac{\text{area} \times \text{viscosity} \times \text{velocity}}{\text{film thickness}} = \frac{S\eta V}{D} \qquad (1)$$

For complex fluids, the viscosity is a complex quantity (being frequency or velocity dependent), and the shear forces are usually described by the WLF equation[1] in terms of the storage and loss moduli, G' and G''

$$G' = \omega\eta'' \qquad G'' = \omega\eta' \qquad (2)$$

where single and double primes refer to the real and imaginary parts, respectively, of η and G. In this formalism, strain amplitudes are generally small, the applied normal load L or pressure P does not usually enter into the equation, and no yield points or shear-induced phase transitions are allowed. Thus, while rheological measurements are usually done at different driving frequencies, different (but small) amplitudes and temperatures, and constant pressure, friction measurements are normally done at constant velocity, large amplitudes, and constant temperature, but different loads. Rheological measurements anticipate that a sinusoidal input will result in a sinusoidal output, whereas tribological measurements anticipate a roughly constant output or a stick−slip response. Only in the thick film regime, corresponding to the bulk limit, do the two approaches truly converge, as described by eq 1 for two planar surfaces.

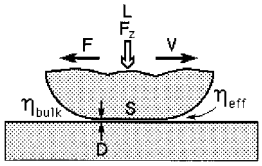

Figure 1. Couette-flow geometry and also the geometry of two shearing surfaces in a surface forces apparatus (SFA) under an applied load.

Aims of the Experiments. We have chosen to study a "complex fluid" rather than a "simple liquid" for which there is now an extensive literature, both experimental and theoretical,[2−6] and have therefore focused our attention on a polymer melt—PBD of MW ≈ 7000 g/mol—that is above the entanglement MW and already non-Newtonian and viscoelastic in the bulk state. This is not to say that simple liquids behave in a simple way under confinement, quite the contrary: recent studies by Gee *et al.*[7] and Granick *et al.*[8−10] on spherical and short-chain molecules such as alkanes, octamethylcyclotetrasiloxane (OMCTS) and low MW polymer melts have shown that when confined in films less than 2.5−5.0 nm thick, they cease to behave as bulk liquids.[9] In some cases the transition is abrupt, like a first-order phase transition, from a liquidlike (shear melted) state to a solid-like (frozen) state with increasing confinement. In others, the viscosity and molecular relaxation times increase continuously to very high values, up to 7 orders of magnitude higher than the bulk values, according to

$$\eta_{eff} \propto \dot{\gamma}^n \qquad (3)$$

where $\dot{\gamma}$ is the shear rate ($\dot{\gamma} = V/D$ for Couette flow), and where n has been found to vary between 0 and −1.0 in the transition.[8−13]

The aims of these experiments were (i) to expand the dynamic force-measuring technique of the SFA to enable higher sliding speeds and shear rates to be studied, (ii) to study the full range of dynamic properties of a complex fluid film, especially the transition from pure

† Now with Institute of Polymer Research, P.O. Box 120411, D-01005 Dresden, Germany.

[⊗] Abstract published in *Advance ACS Abstracts,* March 15, 1997.

S0024-9297(95)01912-7 CCC: $14.00

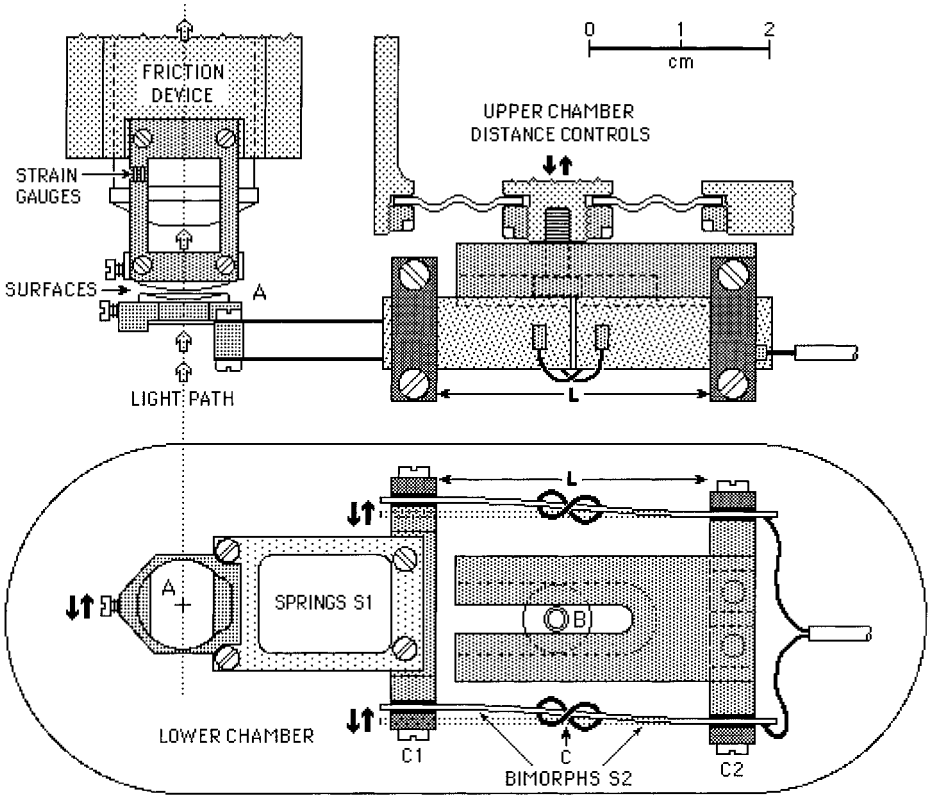

Figure 2. New sliding attachments introduced to the SFA 3 for shear and friction experiments. The bimorph slider is a displacement transducer allowing for steady, sinusoidal, or triangular motion of the lower surface over a large range of distances (up to 1 mm) and frequencies (from 10^{-6} Hz to 200 kHz). The friction device measures the friction forces produced on the upper surface via four semiconductor or resistance strain gauges. It is also a displacement transducer, allowing for the top surface to be moved at various velocities over a distance of up to 5 mm. The top and bottom surfaces are here shown aligned, but in practice the friction device may be rotated about a vertical axis before being attached to the apparatus so that the top surface can move at any chosen direction in the horizontal plane.

bulk to pure frictional behavior, and (iii) if possible, to develop a general scaling formalism or constitutive relations that effectively describe this transition, one that encompasses the WLF equation for bulk flow at one extreme, and Amontons' law of friction

$$\mu = \frac{\text{friction force}}{\text{applied load}} = \frac{F}{L} \tag{4}$$

where μ is a constant independent of velocity, or some other equation of boundary and interfacial friction, at the other.

Experimental Section

Materials: PBD Polymer Melt. We have chosen the previously well-characterized polymer melt polybutadiene (PBD) of chemical structure $(-CH_2-CH=CH-CH_2-)_n$. Polybutadienes are available in a large range of molecular weights and their bulk rheological properties have been described by Colby *et al.*[14] We used a PBD sample of $M_w = 6950$ which is above the molecular entanglement weight of $M_e = 1850$, thereby ensuring viscoelastic polymer-like rather than simple liquidlike properties already in the bulk. The PBD 7000 sample was monodisperse ($M_w/M_n = 1.03$), but the polymer was not completely linear or isomorphous: there was 9% vinyl branching and a random distribution of cis (34%) and trans (57%) C=C bonds. Other relevant parameters are $R_g = 3$ nm and $\eta = 50$ P (5 Pa s) at 25 °C. All the experiments were done with a droplet of polymer inserted between the two mica surfaces. Due to the susceptibility of PBDs to cross-link when exposed to light and oxygen, we took special care to ensure that all measurements were done in an inert atmosphere of dry nitrogen gas and in the presence of P_2O_5 desiccant. No degradation in the sample properties (for example, an increasing viscosity with time due to cross-linking) was seen during the time of the experiments.

New SFA Attachments for Shearing Experiments. The forces between mica surfaces were measured using a surface forces apparatus (SFA 3) described by Israelachvili and McGuiggan.[15] New sliding attachments introduced to the SFA 3 for shear and friction experiments are shown in Figures 2 and 3. These attachments, which are described in the following section, allow for simultaneous lateral sliding and normal (perpendicular) motion of the surfaces at the same time as both the lateral (shear) and normal forces are measured. In addition, the surfaces may be imaged using the FECO optical interference technique, which gives the surface separation and a direct visualization of the local surface geometry at all times during dynamic interactions.

Attachment for Moving the Lower Surface: Bimorph Slider. The lower surface is supported at the end of a double-cantilever spring (Figure 2—S1) used for measuring the normal forces between the surfaces, as previously described.[15] Lateral movement is accomplished with two (or—for increased driver stiffness—four) parallel piezoelectric bimorph strips **S2**. Bimorphs are "piezoelectric couples" made of two thin sheets of piezoelectric ceramic bonded together by a thin layer of hard conducting material. The two outer faces of each bimorph are coated with thin conducting layers of metal (usually silver or nickel), which provide protection and serve as suitable electrode surfaces for electrical connections, such as the soldering of connecting wires. Before two piezoelectric sheets are bonded to form a bimorph, their polarity is reversed relative to each other, so that when a dc voltage is applied across the bimorph, one sheet expands lengthways as the other contracts, resulting in a net bending of the bimorph. For low applied voltages (<100 V) the bending, or lateral displacement of each end, is proportional to the applied voltage V. Bimorphs are capable of producing much larger displacements than piezoelectric crystals for the same applied voltage. Bimorphs also work in

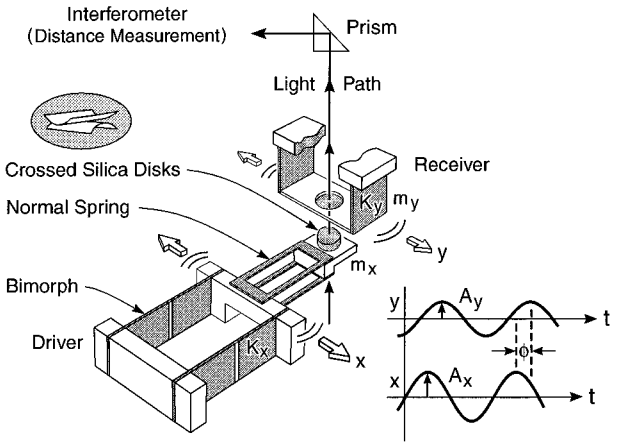

Figure 3. Shear elements of the dynamic surface forces apparatus. The lower surface rests on a normal spring that is attached to two piezoelectric bimorph strips of stiffness K_x which bend according to the input voltage signal. The upper surface movement is coupled to the lower through the liquid film between them. Strain gauges detect the corresponding bending of the springs K_y. The vibration amplitudes A_x and A_y and phase delay ϕ characterize the rheological properties of the liquid. The surface shape and gap or film thickness is continuously monitored by an optical interferometric technique.

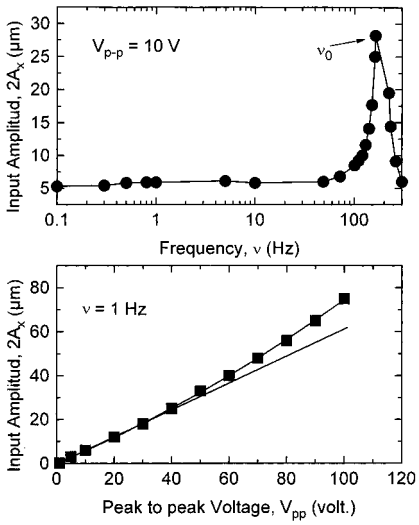

Figure 4. Input voltage−input displacement (V_{p-p} − A_x) calibration curves of the bimorph slider shearing element. Top: A_x as a function of the driving frequency ν at a constant ac voltage of V_{p-p} = 10 V. Bottom: A_x *vs* the driving voltage V_{p-p} at a constant frequency of ν = 1 Hz. The sharp increase of the amplitude at $\nu \approx 200$ Hz corresponds with the resonance frequency of the slider.

reverse, as force sensors. Thus, when a force is applied to one end, a large voltage develops across the two outer electrode faces, which can be easily measured. Bimorphs have long been used in SFA force measurements, both as displacement transducers and as force sensors.[6,16,17] The bimorphs used here were PZT 4, 0.023 in. thick, silver coated, from Morgan Matroc Corp.

To convert the pure bending motion of a bimorph into a linear displacement, one may create a "sectored" bimorph by scraping away a thin strip of the conducting metal coat from the center of each face **C** and then electrically connecting the two pairs of diagonally opposite faces as shown in Figure 2. This splits the direction of the applied voltage across the halves (sectors) of the bimorph, making each half bend in the opposite direction. If the halves are of equal length, the resulting effect is a pure linear displacement of the two ends relative to each other, just as occurs with a double-cantilever spring, with no net rotation or bending component. By using two or more parallel bimorphs in this way, a highly robust linear displacement transducer is produced, and this mechanism was used to drive the lower surface, as shown in Figure 3. In addition, normal vertical motion of the whole slider assembly and lower surface **A** is produced by a three-stage mechanical translation mechanism composed of micrometers and springs located in the upper chamber. This has been described in detail by Israelachvili and McGuiggan.[15]

The active length, **L**, of the sectored bimorph can be adjusted by moving the two clamps, **C1** and **C2**, closer or farther apart. This changes the stiffness of the bimorphs (in proportion to $1/L^3$). The increased stiffness or decreased L also results in a decreased range of travel for a given applied voltage (proportional to L^2), and to an increased natural frequency of the lower surface "drive" (proportional to $1/L^{3/2}$). Since the two clamps, **C1** and **C2**, have to be spaced symmetrically about strip **C**, changing the clamping positions also changes the horizontal position of the lower surface, **A**. To keep the horizontal distance **A**−**B** constant, the whole bimorph mount may be relocated by shifting it to the left or right and then relocking it to the upper chamber with screw **B**.

Lateral motion of the lower surface **A** is produced by applying a dc or ac voltage to the bimorphs through a coaxial cable connected to the outside of the lower chamber via a Teflon-sealed Lemo-type connector. In most cases, it is desirable to have a "drive" that (i) can travel over a large distance, (ii) is very rigid (stiff), and (iii) has a high natural frequency (see Theoretical Section below). For a typical PZT bimorph of active length L = 30 mm, the range of travel (at ±100 V dc across the bimorph) is about ±50 μm, and the stiffness of a double-bimorph slider is $K_x \approx 10^4$ N/m (Figure 3). The effective mass of the lower surface support or "drive" is $m_x \approx 8$ g, which determines the upper limit for dynamic measurements (corresponding to the resonant frequency of the drive) at approximately $\nu_x \approx (1/2\pi)(K_x/m_x)^{1/2} \approx 200$ Hz. Higher travel distances, up to 1 mm p−p, can be attained by increasing the active bimorph length, L, using clamps **C1** and **C2**, but at the cost of a decreasing stiffness. Alternatively, higher stiffnesses K_x and resonant frequencies ν_x can be attained by reducing the active bimorph length, but this also lowers the travel distance for a given (maximum safe or linear) voltage. Thus, some compromise is always required. The ability to readily change the active bimorph length provides sufficient flexibility for optimizing the system parameters for most types of experiments. The mechanical characteristics of the drive are illustrated in Figure 4.

In sliding experiments, it is often desirable to have surfaces moving (shearing) at some *constant* speed or shear rate rather than sinusoidally. This can be achieved with the bimorph slider by applying a triangular voltage signal. This produces constant velocity motion in one direction until the turning point and then in the reverse direction, repeatedly. In this way, very low or very high constant velocities can be achieved. For example, using the above operating parameters (L = 30 mm), the range of practical speeds attainable using a function generator that provides a 1−100 V p−p triangular signal (corresponding to 0.7−70 μm total travel per cycle) is from 0.1 nm/s at a driving frequency of $\nu = 10^{-6}$ Hz to 10 mm/s at $\nu = 10^2$ Hz. For a film thickness of 10 nm, these speeds correspond to shear rates that can be varied from $\dot{\gamma} = 10^{-2}$ to 10^6 s^{-1}—a range of 8 orders of magnitude.

Finally, since bimorphs can both induce and detect motion, the bimorph slider may also be used as a friction force-measuring spring, although we have not used it in this way in these experiments.

Attachment for Measuring Friction Forces. The friction force-measuring attachment, or "friction device", is similar to one previously described for use with the SFA Mk 2.[18] It has been modified for use with the SFA 3, and is also shown in Figure 2 and, more schematically, as the "receiver" in Figure 3. Four strain gauges are attached symmetrically to two oppositely bending surfaces of the vertical double cantilever friction spring. These make up the four arms of a Wheatstone bridge which is used to measure the lateral displacement produced on the upper surface by the motion of the lower surface. The resistance strain gauges used in the previous

friction device,[18] have been replaced by semiconductor strain gauges, which are 100 times more sensitive. The mass m_y of the upper surface or "stage", and the dimensions of the friction force-measuring springs (length, width, and thickness), can be optimized to provide (i) high force sensitivity (bridge output voltage *vs* friction force), or (ii) high displacement sensitivity (bridge output voltage *vs* lateral displacement), and (iii) high natural frequency ν_y of the "stage". The latter property is desirable for obtaining a high dynamic range and the ability to measure rapid transient effects such as stick-slip friction. Typical optimum values used were $K_y \approx 10^3$ N/m, $m_y \approx 2.2$ g, and $\nu_y \approx 120$ Hz. When used with a strain gauge amplifier (MEASUREMENTS GROUP, Model 2311) and chart recorder (SOLTEC, Model 1242) or storage scope recorder (TEKTRONIX, Model 2232), the dc friction force sensitivity is about $\sim$50 μN ($\sim$5 mg), which corresponds to a lateral displacement of the friction spring of 5 nm. Even greater sensitivities can be obtained when measurements are made in ac mode with a lock-in amplifier (Stanford Research Systems digital two-phase lock-in amplifier Model SR830) which also allows independent measurements of the in-phase and out-of-phase components of the output signal. In principle, it should also be possible to measure the motion of the friction spring using a capacitance or optical technique, for example, laser light interferometry, instead of strain gauges. Strain gauge measurements of spring deflections do not have the sensitivity of capacitance or optical techniques but they do have the advantage of fast response times and simplicity of construction and use. Capacitance measurements introduce unwanted forces between the plates, and in common with optical interferometric techniques loses sensitivity when used over large distances ($D \gg \mu$m).

The friction device also has the capability of driving the upper surface (the stage) at a constant speed using a mechanical drive that is powered by a variable speed dc motor with an encoder readout.[18] The total distance of travel is much larger than can be attained with bimorphs: $\sim$5 mm instead of 0.1−1 mm. However, the range of sliding speeds attainable is more limited, and sinusoidal motions are not feasible. Nevertheless, when used in this way, the upper friction attachment serves as a complete, self-contained unit, capable of both generating movement and measuring the resulting friction forces. The lower (bimorph) attachment is only capable of generating movement, and so must be used in combination with the friction device whenever friction forces need to be measured as well.

It is also possible to use the bimorph slider as a displacement sensor, recording the output voltage produced by the bimorphs when they are disturbed. When used in this way, the motor on the friction device is used to move the upper surface (which now becomes the drive), and the lower surface now becomes the stage. This setup is not as practical as the first one described above because the motor cannot provide ac motion and piezoelectric bimorphs, because they are lossy, are unreliable as dc sensors at low frequencies or driving speeds.

Equations of Motion. When undergoing forced oscillations, the mechanical system may be described in terms of two coupled, damped, forced harmonic oscillators (Figure 5, top)

$$m_x\ddot{x} + K_x x + \kappa_x\dot{x} + \kappa(\dot{x} - \dot{y}) = F_0 e^{iwt}$$

$$m_y\ddot{y} + K_y y + \kappa_y\dot{y} - \kappa(\dot{x} - \dot{y}) = 0 \qquad (5)$$

where $(x - y)$ is the relative lateral displacement of the lower and upper surfaces. The subscripts x and y refer to the **drive** (bimorph slider) and **receiver** (stage and strain gauges), F_o is the driving force, and $\kappa(\dot{x} - \dot{y}) \equiv \kappa V = F$ is the real friction force between the two surfaces defined in terms of κ, the damping of the lubricating fluid between the two surfaces. The coefficient κ contains all the information on the friction force between the surfaces and thus depends on the geometry of the surfaces and on the relative velocity V, and for non-Newtonian lubrication it will also depend on other factors such as time and previous history. At periodic driving frequencies $\omega = 2\pi\nu$ much lower than the resonance frequencies ω_o of the drive and receiver the inertial terms $m_x\ddot{x}$ and $m_y\ddot{y}$ can be

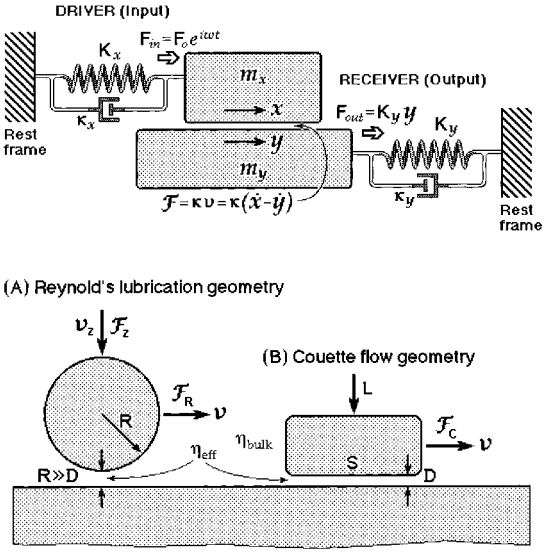

Figure 5. Equivalent mechanical circuit for the modified SFA (top). The geometry of the surfaces determines the hydrodynamics of the problem: (A) sphere on flat, described by eqs 10 and 11; (B) flat on flat, described by eq 13.

neglected. Likewise, we may neglect the two independent damping terms of the drive and stage, κ_x and κ_y, which are both much less than κ, and mainly affect the amplitude of the oscillations close to resonance ($\omega \approx \omega_o$). The glue layers supporting the substrate surfaces are generally much more rigid than the other compliant parts of the system and their contributions are automatically incorporated into K_x and K_y. If required, this contribution can be independently calibrated with the two surfaces rigidly clamped together with a metal rod. If the stiffness of the bimorph drive K_x is greater than that of the friction force-measuring spring K_y ($K_x > K_y$) the above equations simplify to

$$x = (F_0/K_x)e^{iwt} = A_0 e^{iwt}$$

$$K_y y - \kappa V = 0 \qquad (6)$$

The forced movement of the lower surface x is thus transmitted via the friction force to the upper surface where it is measured by the strain gauges as a displacement, y (Figure 3). The oscillatory response is of the form

$$y = A_y \exp[i(\omega t + \phi)] \qquad (7)$$

where the amplitude and phase of the upper surface are given by

$$A_y = \frac{A_0}{[1 + K_y^2/(\omega^2\kappa^2)]^{1/2}}$$

$$\tan\phi = -\frac{K_y}{\omega\kappa} \qquad (8)$$

From the above, the damping coefficient is given by

$$\kappa = \frac{K_y}{\omega[(A_0/A_y)^2 - 1]^{1/2}} = \frac{K_y}{\omega\tan\phi} \qquad (9)$$

We may note that all the parameters on the rhs of the above equations are known or directly measurable. The above solution is similar to one which applies to two surfaces undergoing normal vibrations along the z-direction.[6] The main difference between normal and shearing motion is in the damping coefficient, κ, which depends on different surface geometry parameters (grouped in Ω) and the viscosity (Figure 5). For example, for a sphere moving towards or away from a flat surface in a simple Newtonian liquid with shear viscosity η (Figure 5A), we have[19]

$$F = \kappa v \equiv \Omega \eta v = 6\pi R^2 \eta v/D \tag{10}$$

whereas for a (non-rotating) sphere moving parallel to a flat surface surface[20−22]

$$F = \kappa v \equiv \Omega \eta v = 6\pi R \eta v \left[\frac{8}{15}\log\left(\frac{2R}{D}\right) + ...\right] \tag{11a}$$

$$\approx \frac{16}{5}\pi R \eta v \log\left(\frac{2R}{D}\right) \qquad \text{for } R \gg D \tag{11b}$$

where R is the radius of the sphere and D is the closest distance of separation in both cases. For two crossed cylinders, the geometry adopted here, the effective hydrodynamic radius R is related to the cylinder radii R_1 and R_2 by[23]

$$R^2 = 2(R_1 R_2)^{3/2}/(R_1 + R_2) \tag{12}$$

when $R_1 = R_2$, we may put $R = R_1 = R_2$ and the geometry is equivalent to a sphere of radius R near a flat surface.

Another important geometry that was also studied is that of two flat parallel surfaces (Figures 1 and 5B). If one surface of area S is moving laterally past the other at a fixed surface separation D, the situation corresponds to Couette flow and the viscous force is given by[24]

$$F = \kappa V \equiv \Omega \eta V = \frac{\text{area} \times \text{viscosity} \times \text{velocity}}{\text{film thickness}} = \frac{S\eta V}{D} \tag{13}$$

We should emphasize again that the above relations hold only for Newtonian fluids. In some cases, when film thicknesses approach molecular dimensions and fluids cease to be Newtonian, we shall use the above equation to compute an effective viscosity, η_{eff}, defined by

$$\eta_{\text{eff}} = FD/SV \tag{14}$$

where all the parameters on the RHS are measured values.

If we deal with a viscoelastic liquid, the viscosity η_{eff} may be represented by a complex function[1] $\eta_{\text{eff}} = \eta' - i\eta''$ where η' is the viscosity component that is in phase with the rate of strain, and η'' is the component that is 90 degrees out of phase. Solving eq 6 for the case of linear viscoelasticity, we obtain

$$\eta' = \frac{K_y f \sin\phi}{\omega\Omega[f^2 - (2f\cos\phi - 1)]}$$

$$\eta'' = \frac{K_y(f\cos\phi - 1)}{\omega\Omega[f^2 - (2f\cos\phi - 1)]} \tag{15}$$

where $f = (A_0/A_y)$. The magnitude of the viscosity is given by

$$\eta = \sqrt{\eta'^2 + \eta''^2} = \frac{K_y}{\omega\Omega[f^2 - (2f\cos\phi - 1)]^{1/2}} \tag{16}$$

and the "storage" and "loss" shear moduli are, respectively[1]

$$G' = \omega\eta'' \qquad G'' = \omega\eta' \tag{17}$$

which together define the complex effective shear modulus $G_{\text{eff}} = G' + iG''$. We should note that $\eta''$and G' are proportional to the energy stored elastically in the system, whereas η' or G'' are proportional to the energy lost per cycle through irreversible viscous (thermal) dissipation. When the viscosity and shear modulus are different from the bulk values, as occurs in thin films, the "effective" viscosity, η_{eff}, and shear modulus, G_{eff}, as measured by use of the hydrodynamic equations 10−14 and defined by eqs 16 and 17 will be used instead of η and G in all of the above equations. This is the same approach as that used by Granick and co-workers for non-Newtonian confined fluids.[9]

It is also useful to know the shear rates, the shear strains, and the shear stresses. When using sinusoidal signals the shear rate can be calculated from

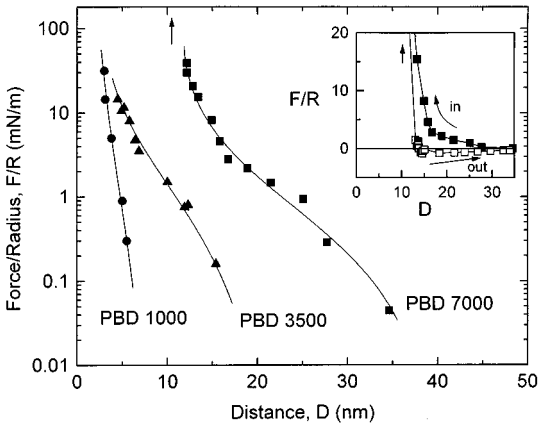

Figure 6. Force runs of polybutadiene samples of different molecular weights (See Table 1). The "hard wall" at D ≈ 10 nm, shown by the vertical arrows, can be visualized better in the inset, which also shows the hysteresis in the approach (compression) and separation (decompression) paths.

$$\dot\gamma = \frac{V}{D} = \frac{i\omega[A_0 - A_y\exp(i\phi)]\exp(i\omega t)}{D} \tag{18}$$

In general, we will refer to the maximum shear rate, given by

$$\dot\gamma = \frac{\omega\sqrt{(A_y\sin\phi)^2 + (A_0 - A_y\cos\phi)^2}}{D} \tag{19}$$

Using eq 16, this can be transformed into

$$\dot\gamma = \frac{K_y A_y}{\eta\Omega D} \tag{20}$$

The maximum shear strain, γ, is consequently

$$\gamma = \dot\gamma/\omega \tag{21}$$

It is now straightforward to calculate the maximum shear stress, σ, imposed on the sample using the general viscoelastic relations:

$$\sigma \equiv F_0/S_{\text{eff}} = \eta_{\text{eff}}\dot\gamma \tag{22}$$

Equation 22 allows us to calculate an effective area of shear, S_{eff}, in any geometry.

All the above equations assume a linear response, viz., that y is directly proportional to x, so that a sinusoidal input produces a sinusoidal response, which is generally the case for small strains[1,25] and in the absence of yield points which can occur in the tribological regime. They also assume that the viscosities η' and η'', and shear moduli G' and G'' depend only on the frequency and not on the amplitude of the stress or strain,[25] which was indeed borne out by the measurements on the thicker films (see Figure 8A later).

Results and Discussion

Static Forces. The normal force between two mica sheets across PBD 7000 at 25 °C is shown in Figure 6. The force has been normalized by the radius of curvature, R. Figure 6 also shows previous results obtained with PBD 3500 and PBD 1000 of lower molecular weights.[26] The relevant physical characteristics of the PBDs are listed in Table 1.

The static forces were measured slowly, to allow for restricted mechanical equilibrium to be reached at each separation. For PBD 7000, the time to equilibrate at each separation shown in Figure 6 was at least 2−3 min, and several forces run with longer time intervals between measurements showed no discernible change. It should be noted, however, that true thermodynamic

Table 1. Interaction Properties of Adsorbed Polybutadiene (PBD) Layers[a]

Property	PBD 1000	PBD 3500	PBD 7000
Polydispersity (M_w/M_n)	1.08	1.16	1.03
no. of segments per chain	20	65	129
MW (g/mol)	1000	3500[c]	6950[c]
R_g in the bulk (nm)	1.2	2.2	3.0
decay length of measured force (nm)[b]	0.9	2.9	4.0
hard wall per surface (nm)[b]	1.5	1.9	5.0

[a] Data for PBD 1000 and PBD 3500 from ref 31. [b] Maximum errors in distance values: ±20%. [c] Above the entanglement MW of 1850 g/mol.[14]

equilibrium is probably not attained in these experiments—the polymer remains between the two surfaces and does not get squeezed out into the bulk as expected theoretically. In theoretical treatments of polymer interactions, this type of equilibrium is commonly referred to as "restricted" or "partial" equilibrium,[27] where it is assumed that "equilibrium" is attained in the gap under the conditions of constant amount of polymer, that is, with no exchange allowed with polymer in the bulk "reservoir". We note that the tail end of the force profiles are different on approach and separation (Figure 6, inset). This type of irreversibility, where the approach is more repulsive than the separation, may reflect a true hysteresis effect in the interaction, but it could also be due to the finite rates of approach and separation which may not be sufficiently slow to totally eliminate all the viscous drag forces.[28] In the latter case, the true restricted equilibrium interaction would be expected to fall somewhere in between the approach and separation curves shown in Figure 6. However, the "hard wall" at $D \approx 10$ nm (vertical arrows) is not expected to be due to viscosity forces, but to the restricted equilibrium nature of the interaction.[29]

Figure 6 shows that the static forces are essentially overall repulsive (with a possible small adhesion at $D \approx 10$ nm). There are two regimes: a steeply repulsive force with an incompressible "hard wall" at $D \approx 10$ nm, and a roughly exponential decay at larger distances. For PBD 7000 the exponentially decaying region has a decay length of about 3.5 nm, which is close to the radius of gyration of PBD 7000, $R_g = 3$ nm. Similar trends were found in the previous study with lower MW PBD[26] (Table 1). These purely repulsive forces appear to follow the restricted equilibrium type of interaction proposed by de Gennes for "pinned" polymer melts[30] and more generally by the Scheutjens and Fleer theory.[27] They indicate strong binding of the polymer to the surface, at least over the time scales of the force runs (1−2 h), and an immobilized layer of thickness ~5 nm, or about $1.5R_g$ per surface. This, too, is consistent with the previous studies on lower MW PBD melts.[26] The chain conformations in such confined surface layers are not known, but have been suggested to be in the glassy or rubbery state.[9,31] In addition, we do not find any short range oscillations as is theoretically expected[32] and previously seen across liquid alkanes and polydimethylsiloxane (PDMS) melts.[28,33] The absence of a short range oscillatory force has also been noted before for PBDs[26] and other adsorbed polymer layers and is most likely to be due to the difficulty of ordering branched polymer chains between two surfaces.[7]

In Table 1 we compare the present results with those obtained previously on PBD 1000 and PBD 3500;[26] it is clear that the short-range forces scale reasonably well with R_g, but not so well with MW. It may also be relevant to note that PBD 7000 and PBD 3500 are above the entanglement molecular weight, $M_e = 1850$, which may act to extend the range of the forces.

Theoretically, the issue of the forces between surfaces across polymer liquids has been clouded by questions of equilibrium vs "partial", "limited", or "restricted" equilibrium. Under true equilibrium conditions between a confined polymer melt and the bulk reservoir, de Gennes, using scaling theory,[30] and Scheutjens and Fleer using mean-field theory,[27] have predicted a monotonic attraction at all separations down to contact (zero separation), although the last layer of strongly adsorbed segments may not be removed, even at equilibrium.[27] Under conditions of restricted equilibrium, the same theories predict a repulsion at all separations. In both cases the interaction is expected to have a range of a few R_g. Experimentally, only repulsive forces have been measured across PBD melts.[26,34,35] In contrast, the forces across straight chained, unbranched PDMS melts are oscillatory[33] without the long-ranged monotonically repulsive component,[28] in agreement with molecular theories and computer simulations.[32] More recent results with PPMS (polyphenylmethylsiloxane) melts[31] suggest that the monotonic long-ranged repulsion is stable over long time periods (24 h), and that the very act of compressing the adsorbed layers to measure the forces between them acts to further extend their relaxation time.

In all the results reported so far, time effects have played an important role, and in this regard it is worth noting that the forces between two surfaces in a polymer melt are often very similar to those of polymers adsorbed from solution,[36] where in both cases the interactions occur at fixed amount of adsorbed, pinned or tethered chains, that is, at "restricted equilibrium" even over surprisingly long time periods.

Dynamic Forces. Three Dynamic Regimes. As discussed in the Introduction, three dynamic regimes—bulk, transition or intermediate, and tribological—can be distinguished as a liquid film progressively thins. These produce characteristically different output (response) curves for a given input signal, as illustrated by the typical friction traces shown in Figure 7. Figure 7A shows a typical calibration curve for the input (bimorph slider drive) and output (friction spring strain gauge response) as recorded by an oscilloscope for surfaces of radii $R = 2$ cm separated by $D = 250$ nm of PBD 7000 and subjected to 6.5 Hz oscillations. We used sinusoidal signals to study the thick-film regime, as is commonly done with conventional rheometers. We may note the sinusoidal response of the receiver, but with a phase delay of 82°, due to the bulk (intrinsic) viscoelastic properties of the polymer melt. In all the dynamic experiments reported here, the maximum voltage applied to the bimorph elements was ±20 V (40 V p−p), corresponding to about ±15 μm displacement, which is well within the linear regime of the bimorph slider (cf. Figure 4).

Concerning the linearity of the response (y) to the sinusoidal input (x), in the bulk regime (Figure 7A) this was found to be linear[25] for shear strains $\gamma = |x - y|/D$ up to about 10, above which both G' and G'' increased with increasing driving amplitude (Figure 8A). From data such as shown in Figure 7A obtained in the linear regime we may calculate η', η'', G', and G'', using eqs 15 and 17. The results are presented in Figures 8B and 9.

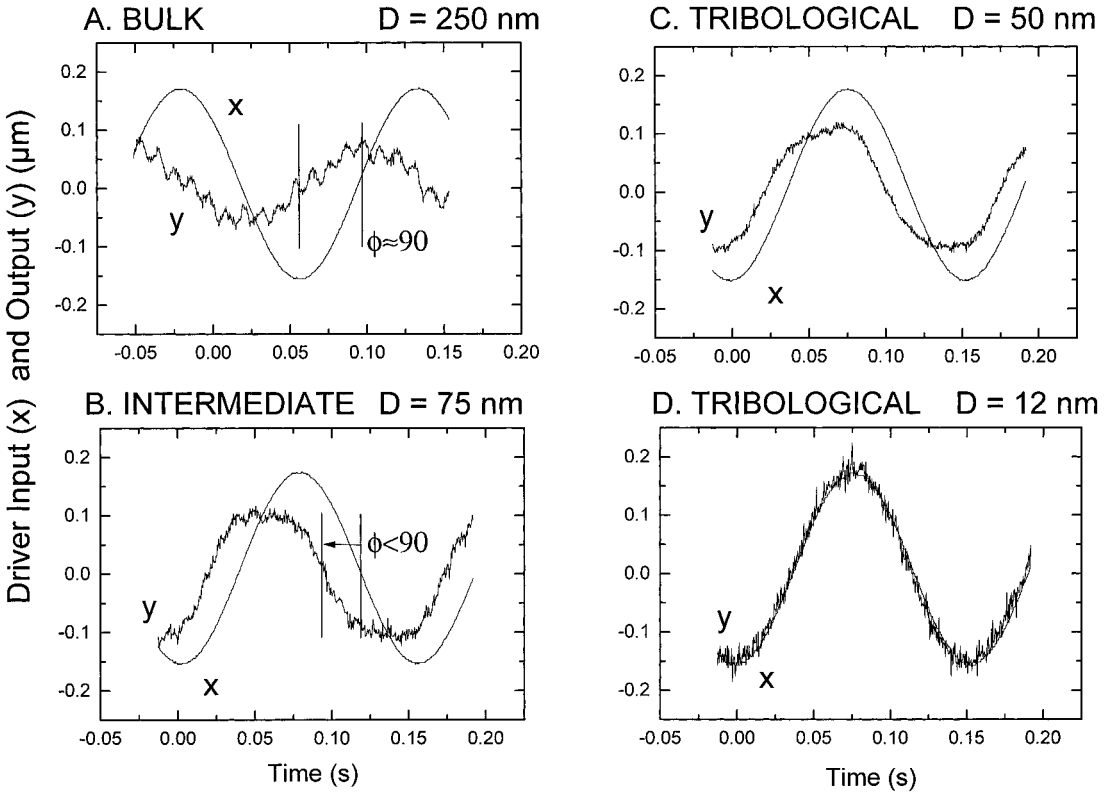

Figure 7. Typical friction traces from the oscilloscope showing the displacement of both surfaces x and y. The experimental conditions are $R \approx 0.02$ m, $\nu = 6.5$ Hz, and $T = 25$ °C. The traces were recorded at the surface separations indicated. (A) The shift between the two sinusoidal waves is $\phi = 82°$, corresponding to a purely viscoelastic character. In this regime the response was linear[25] up to strains of $\gamma = |x - y|/D \approx 10$ (cf. Figure 8A). (B, C) A sinusoidal input no longer results in a purely sinusoidal output. The plateau region is indicative of a yield point. However, in the intermediate regime (B), the response was close to linear[25] for strains $\gamma < 0.3$, and these were the values used for determining the effective viscosities and shear moduli of the confined films displayed in Figures 8−12. (D) Small amplitude oscillations in the tribological regime where the yield point is never reached due to the greatly increased friction force.

In the intermediate regime, and particularly in the tribological regime, the response became increasingly and intrinsically nonlinear, even for small strains. In the intermediate regime, we therefore use the effective values η_{eff} and G_{eff} defined by eqs 14−17 to describe the rheological properties of the films, as described above. Parts B and C of Figure 7 show the quantitatively different and increasingly nonbulklike and nonlinear responses obtained for progressively thinner films. The responses at this frequency are increasingly nonsinusoidal and of decreasing phase angle ϕ, even though the input signal is purely sinusoidal. The flat plateau part of the output corresponds to steady state sliding at constant force and is indicative of a yield point which is characteristic of pure tribological behavior (the flat parts can be seen more clearly when larger shearing amplitudes are applied, as shown later in Figure 14). The flat regions can also have stick-slip spikes superimposed on them whose periodicity is unrelated to the driving frequency.[37] According to eq 1, the constant friction force F of the plateau region in the tribological regime implies that $S\eta V/D = S\eta\dot{\gamma} =$ constant, i.e., in the pure tribological regime

$$\eta_{\text{eff}} \propto \dot{\gamma}^{-1}$$

$$\therefore \text{F} \propto \text{V}^0 \text{ (}F\text{ is independent of }V\text{, as in eq 4)} \quad (23)$$

which may be contrasted with the behavior in the purely Newtonian viscous regime, i.e., in the bulk regime, where

$$\eta_{\text{eff}} = \text{constant, or } \eta_{\text{eff}} \propto \dot{\gamma}^0$$

$$\therefore \text{F} \propto \text{V } (F \text{ increases linearly with } V\text{, as in eq 1}) \quad (24)$$

Bulk Rheological Regime. We first report or results obtained on relatively thick films—the bulk rheological regime. Figure 8 shows the results obtained for PBD of MW 7000. For comparison, the figure also shows previously published rheological data (solid lines) obtained on bulk PBD of MW 1.3×10^5.[14] Both series of curves show the same limiting ω-dependence expected at low frequencies, viz. $G' \propto \omega^2$ and $G'' \propto \omega$, which is typical of bulk polymer fluid in the "terminal zone".[1] Further, the relative magnitudes of G' and G'' scale roughly as expected with the ratio of the MW$^{3.4}$ (ratio $= (1.3 \times 10^5/7000)^{3.4} \approx 3 \times 10^4$) and bulk viscosities (ratio $= 10^5/5 \approx 2 \times 10^4$) of the two liquids: thus, the two sets of curves are shifted by about 3 decades on both the G and ν axes. More specifically, the data for PBD 7000 in Figure 8 exhibit slopes of 0.9 ± 0.1 for G'' and 1.9 ± 0.1 for G', and the computed viscosity is $\eta' = G''/\omega = 3 \pm 1$ Pa s, which is close to but lower than the bulk viscosity of 5 Pa s.[14] The reason for this discrepancy, by a factor of 2, is unknown. One possible explanation is given in ref 14. It is also possible that these films, although relatively thick, are still of submicrometer dimensions and thus may not yet behave as bulk fluids due to either surface-induced deviations such as were observed in a previous study with PDB in thick films at frequencies above 10 Hz[6] and/or due to wall−slip effects[38] which can give rise to a lower effective viscosity

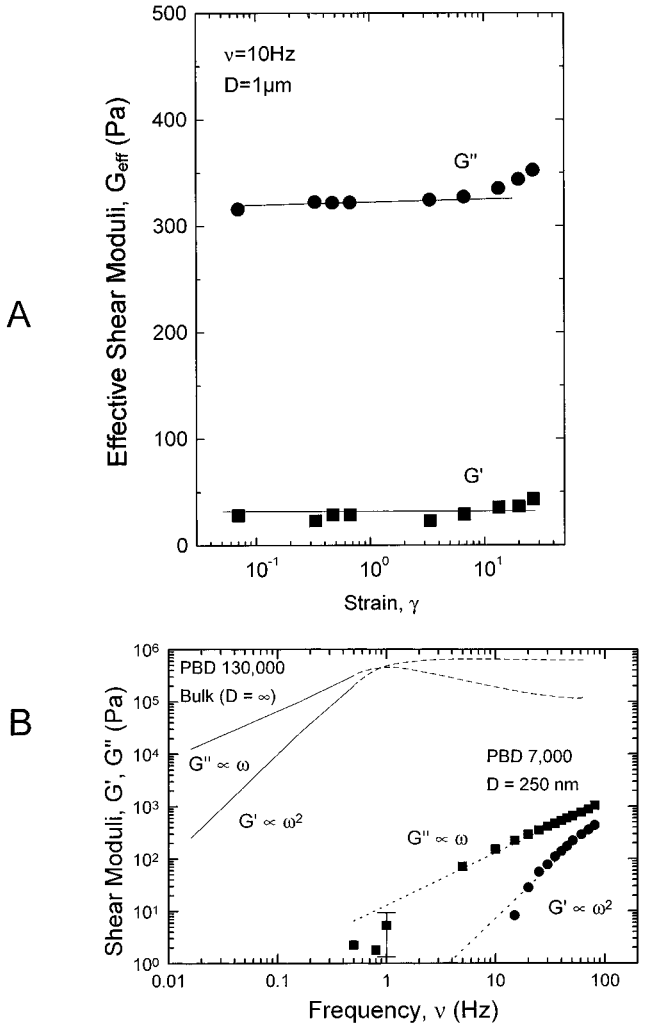

Figure 8. Shear moduli (rheological spectrum) G' and G'' of polybutadiene PBD 7000, (A) *vs* maximum strain $\gamma = |x - y|/D$ at a fixed separation of $D = 1$ μm and frequency $\nu = 10$ Hz, where the response y was proportional to the input voltage x up to strains of ~10, and (B) vs frequency ν at a fixed separation of $D = 250$ nm and strains $\gamma < 1$, which is well within the linear regime.[25] The data were analyzed in terms of eqs 15 and 17. The results correspond to the expected behavior of bulk liquid polymer in the "terminal zone", where $G'' \propto \omega$ and $G' \propto \omega^2$. Data on bulk PBD 130 000 are also shown, taken from ref 14. These thick-film results show that the SFA 3 with the new sliding attachments described here can also be used as a bulk rheometer.

then the bulk value, as was observed here. We note, however, that this discrepancy is insignificant when compared to the order of magnitude changes seen in more confined films.

Transition Regime: Effect of Increasing Confinement. We define the transition regime as that regime where the rheological properties are no longer described by the bulk values, but where the fluid still behaves like a rheological fluid, i.e., where a sinusoidal shear strain input produces a sinusoidal or near-sinusoidal shear stress output. We adopt this definition since it also allows us to clearly distinguish the transition regime from the tribological regime.

Figure 9 shows the shear moduli and effective viscosity of PBD 7000 at different distances D but at a fixed frequency of 13 Hz. We note that G', G'', and η_{eff} remain roughly constant down to a gap thickness of 40 nm, below which they all increase, at first gradually and then much more sharply below 25 nm. This type of

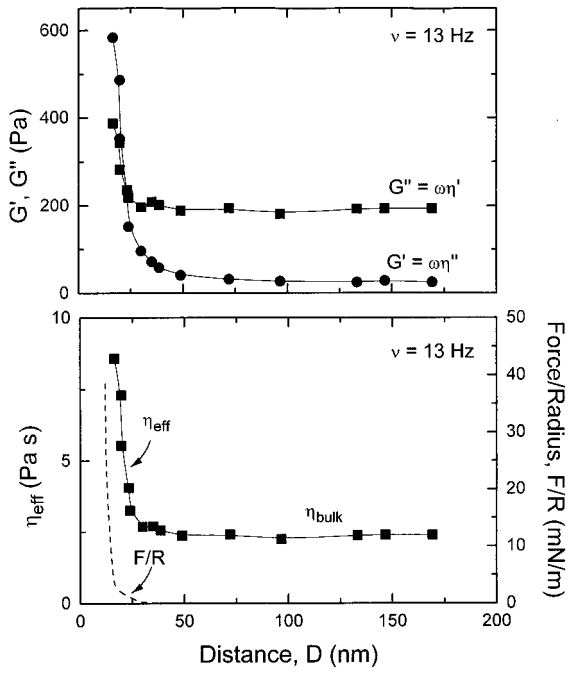

Figure 9. Effect of surface separation D on the shear moduli G_{eff} (top) and effective viscosity η_{eff} (bottom) of polybutadiene at a constant frequency of 13 Hz calculated using eqs 17 and 16, respectively. In this example we eventually observe a crossover of G' and G'' with compression and an increase of the viscosity (see text).

observation has often been interpreted in terms of an immobilized "hydrodynamic" layer at each surface, in this case of thickness $\Delta_H \approx 12$nm, which shifts the shear plane out by Δ_H—a value that might be expected to correspond to the "hard wall" thickness in the force runs described in the previous section. However, $2\Delta_H \approx 25$ nm is more than twice the hard wall thickness of 10 nm obtained with the force runs. Such thicker than expected hydrodynamic layers, extending $2-4R_g$ from each surface, have been observed before both with adsorbed polymers from solution[39] and pinned polymer melts,[6] and are believed to be due to a large contribution coming from the tail ends of adsorbed or pinned polymers.[40]

The data of Figure 9 can be represented more usefully for analysis by plotting $\Gamma = D/\eta_{eff}$ against surface separation D, where

$$\Gamma \equiv \frac{S_{eff}\omega(f^2 - 2f\cos\phi + 1)^{1/2}}{K_y} = D/\eta_{eff} \qquad (25)$$

Thus, a plot of Γ against D should yield a straight line at large D with asymptotic slope equal to the inverse viscosity and which extrapolates back to cut the distance axis at $D = 2\Delta_H$. Figure 10 shows that for PBD 7000 the asymptotic inverse slope (solid line) corresponds to the far-field viscosity of 2.3 ± 0.1 Pa s, and to an intercept at $D = 5 \pm 3$ nm which corresponds to $\Delta_H \approx$ 2.5 nm, which is close to R_g (3.0 nm) per surface.

Thus, depending on the method of interpretation, the hydrodynamic layer thickness Δ_H varies from $\sim R_g$ (when deduced from the far-field viscous forces) to $\sim 2R_g$ when deduced from the static force profiles, to $\sim 4R_g$ (when deduced from the near-field viscous forces). The reason for this large discrepancy is that the concept of a shear rate-independent effective hydrodynamic layer thickness—which also assumes that a totally immobilized layer is followed by a totally bulk like liquid—is a

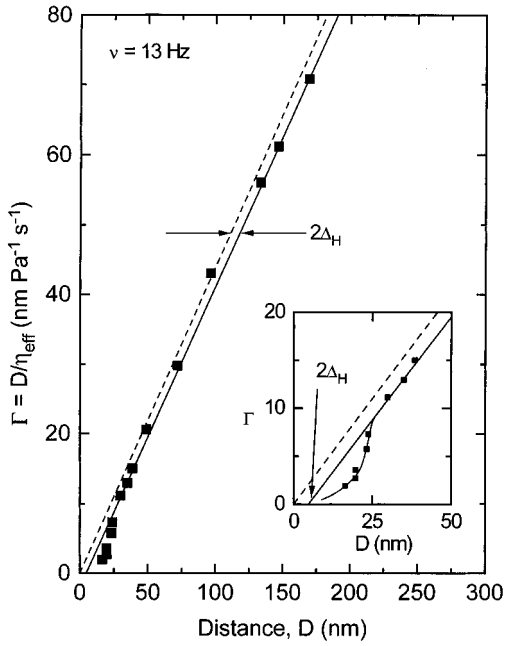

Figure 10. Effective mobility Γ of PBD 7000, where Γ (∝1/η_{eff}) is defined by eq 25 as a function of film thickness *D*. Note the shifting of the straight line from the origin and the bulge on the curve at closer distances. The straight lines correspond to a Newtonian shear viscosity equivalent to 2.3 Pa s. The hydrodynamic layer thickness per surface is $\Delta_H = {}^5/_2 = 2.5$ nm.

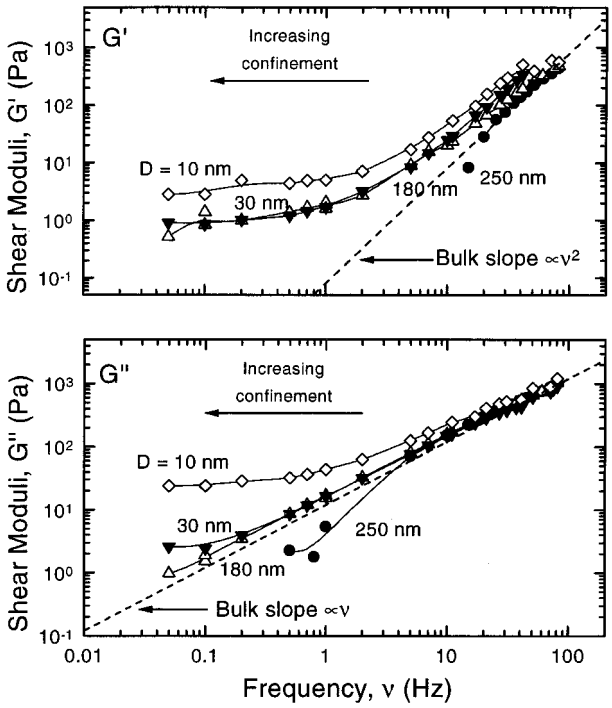

Figure 11. Dependence of the effective shear moduli *G′* and *G″* of PBD 7000 with frequency $\nu = \omega/2\pi$ at 25 °C. The measurements were taken at four constant surface separations *D*.

gross oversimplification and not appropriate for complex viscoelastic fluids. This is because, depending on the frequency or shear rate but also on the distance regime from which the extrapolation in made, quite different values can be obtained. For example, the small bulge occurring below 25 nm in Figure 10 means that a much larger effective Δ_H will be obtained when extrapolating from this distance regime (as was done in Figure 9) than from farther out (as was done in Figure 10). This bulge at small distances is similar to a previously reported bulge that was measured using quite different methods, employing squeeze flow rather than shear flow,[6] and it may reflect some complex rheological behavior of confined polymer fluids over particular distance and shear-rate regimes.[39]

Transition Regime: Effect of Frequency. One of the aims was to obtain the distribution of relaxation times of the confined polymer and, more generally, establish the applicability of the WLF formalism in the transition regime. This can be achieved by measuring the rheological spectrum in this regime. Figure 11 shows the results obtained for G_{eff} (*G′* and *G″*) over the frequency range from 0.1 to 100 Hz at four gap thicknesses from $D = 250$ nm (quasi-bulk regime) to $D = 10-13$ nm (which at small frequencies goes into the tribological regime). Compared to the bulk regime (Figure 8) there is a shift of both *G′* and *G″* towards lower frequencies as *D* decreases. Since the shift in *G′* is more pronounced at any distance *D*, the crossover point of *G′* with *G″* is also shifted to lower frequencies, going from about 200 Hz for the "bulk" sample at $D = 250$ nm to approximately 30 Hz at $D = 10$ nm ($\approx 3R_g$). This indicates a roughly 10-fold increase of the shortest relaxation time from 5 to 30 ms. We may also note the vertical shift in both the *G′* and *G″* curves, especially at lower frequencies, below 5 Hz. This interesting effect indicates an enhancement of the low-frequency contributions to the relaxation spectra and has been previously observed in polyphenylmethylsiloxane (PPMS) melts by Granick and co-workers.[31]

These results show that it is possible to apply a modified WLF approach to confined films to obtain a master curve using a series of curves obtained at constant film thicknesses (as we would at constant temperature or frequency in the WLF case). However the shifts in *G′* and *G″* are not only lateral along the time (frequency or velocity) axis but also vertical, which is more complex than normal WLF shifts, an effect that has also been recently reported in PBD solutions[41] and PPMS melts.[31]

Figure 12A shows the same data (white points), but now plotted as η_{eff} against shear rate $\dot{\gamma}$ on a log−log plot. Such plots have been very useful in analyzing the rheological properties of liquids in thin films, especially in terms of eq 3.[8,9,11,12,42] Figure 12A shows that in films of thickness 250 and 180 nm the shear viscosity remains effectively constant at the bulk value, although a small increase may already be discerned in the 180 nm film. We comment parenthetically that our low shear rate data for thick (250 nm) films had a large error, as indicated by the error bar in Figure 8, which does not allow us to unambiguously conclude that the apparent low rate shear-thinning effect is real. For the thinner films, a striking increase in the viscosity is observed with decreasing shear rate, and below a certain critical value $\dot{\gamma}_c$ the data appear to fall on a straight line ($\eta_{eff} \propto \dot{\gamma}^n$) of slope $n = -0.8 \pm 0.1$. The data shown in Figure 12A appears to be related to the thin-film behavior observed by Granick and co-workers,[8,9,42] except that here we observe a leveling off in the viscosity to occur at *high* shear rates (where it merges with the bulk value) rather than at *low* rates,[9] where η_{eff} is found to also level off but at values that are typically 7−10 orders of magnitude *higher* than the bulk viscosity. This scenario is illustrated schematically in Figure 12B where it is suggested that there is a smooth transition between two plateau regimes; in the transition regime

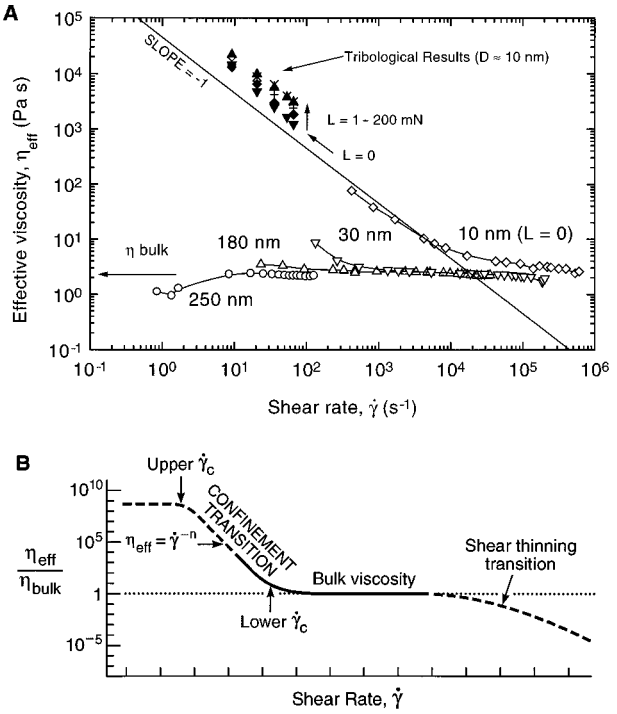

Figure 12. (A) Key: White points, effective viscosity η_{eff} *vs* shear rate, $\dot{\gamma} = d\gamma/dt$, for PBD 7000 at four different surfaces separations, D (same data as in Figure 11); horizontal arrow, measured bulk viscosity;[14] black points, effective viscosity as deduced from the friction experiments at constant sliding velocities. (B) Schematic viscosity−shear rate dependence of fluids in thin films. The confinement transition is absent in bulk samples. Shear thinning transitions often occur in bulk samples and may also occur in thin films at higher shear rates (but were not measured in this study).

between them the effective viscosity varies with shear rate according to eq 3.

The shear thinning transition that is commonly observed with bulk polymer fluids at high shear rates (shown schematically in Figure 12B at large $\dot{\gamma}$) is unlikely to have the same origin as the confinement transition discussed here. The bulk shear thinning transition lowers the effective viscosity below the bulk value *above* some critical shear rate, whereas the confinement transition raises the viscosity above the bulk value *below* some critical shear rate.

Transition Regime: Stress Relaxation Effects. Shear stress relaxations following a large sudden shear strain can be measured using the SFA. This was done by applying a step voltage to the bimorph drive, and recording the resulting stress on the upper surface (the receiver) as a function of time. Such time-dependent transient stresses can also be studied by applying a periodic square-wave voltage input to the bimorph slider. Figure 13 shows some recorded traces for the transient shear forces, F, as a function of time at the two surfaces separations of $D = 180$ nm (Figure 13A) and $D = 30$ nm (Figure 13B). For the thicker film the response is essentially bulk liquidlike, describable by an overdamped viscous liquid undergoing Couette flow. However, the emergence of some nonbulk like behavior is already apparent in these thick films. Thus, for the 180 nm film, immediately after a stepped perturbation, the shear stress at first increases rapidly then relaxes to a low value with a relaxation time of ~0.2 s followed by a much slower relaxation to zero or some small finite value. Thus, at least two relaxation mechanisms—a fast bulk like mechanism and a much slower one—appear to be associated with the cessation of motion.

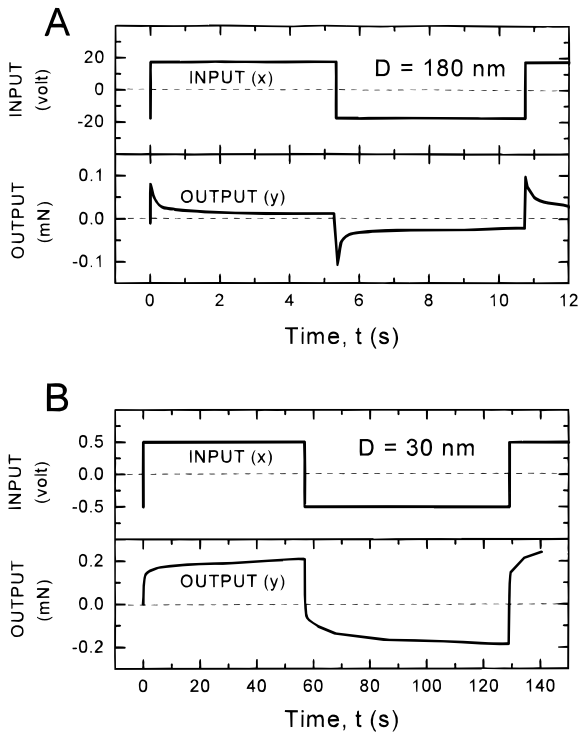

Figure 13. Chart recorder traces of stress relaxation experiments using a square wave input. The figure shows two limiting surface separations: 180 nm (top) and 30 nm (bottom). Note the difference in the time scales.

In contrast, the fluid in the 30 nm film behaves totally differently (Figure 13B): after the rapid initial increase in shear stress following the step function change in voltage, the freezing of the chain dynamics with confinement causes the upper surface to remain stuck to the lower surface for a very long time, even exhibiting some overshoot creep that is almost 3 orders of magnitude slower than the viscous decay displayed by the thicker film (compare the different time scales of parts A and B of Figure 13). The unexpected continuing increase in the stress after the initial fast response may be partly due to creep in the bimorph elements following the step voltage change. However, this effect was not seen in calibration tests made with the surfaces rigidly bonded to each other and subjected to the same step function voltage of ±20 V p−p. One may also note that stress overshoot effects are commonly seen in both tribological and polymer systems, and for polymers they have been described by Ferry[1] in terms of the Voigt−Kelvin element.

Tribological Regime. Experimental Considerations. Friction experiments were performed in a dry atmosphere with a macroscopic droplet of the polymer liquid injected between the surfaces. Before sliding was commenced, the surfaces were usually pressed into flattened contact under a large load, L, so that sliding occurred with the surfaces separated by $D < 15$ nm, stabilized by the steric "hard-wall" repulsion between them (Figure 6). With increasing load, the flattened contact area S increases, following a Hertzian−JKR load−area dependence.[43] The increase in area is due to the elastic deformation of the adhesive glue that supports the mica sheets. Thus, unlike measurements done in the bulk and transition regimes where the applied loads were generally low (essentially zero) and the surfaces remained in their undeformed, rounded state during shear (Figure 5A), in the full tribological regime the shearing surfaces are highly flattened and

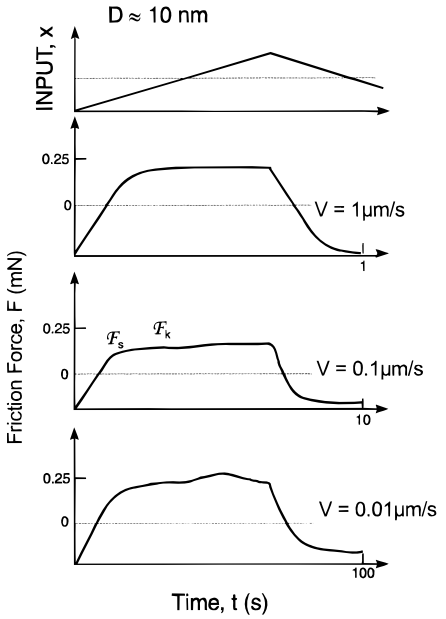

Figure 14. Chart recorder traces of the friction between two mica surfaces separated by a 12 ± 3 nm thick polymer layer of PBD 7000 at three different velocities. The sliding was smooth, exhibiting neither stiction peaks nor stick-slip behavior.

have a Couette flow geometry over the flattened area S (Figures 1 and 5B). Another difference is that tribological measurements generally involve steady state sliding at some fixed drive velocity, V, rather than sinusoidal motion. Back and forth steady sliding over the same area can also be achieved by applying a periodic triangular wave input to the bimorph slider. Note that tribological-type measurements using triangular wave forms may also be carried out on viscoelastic or even simple Newtonian liquids, that is, in the transition and bulk rheological regimes. The difference between conventional rheological and tribological measurements lies more in how the measurements—sinusoidal or steady sliding—are made, which affects the design of the rheometer or tribometer, and how the resulting data are recorded and analyzed; but in principle, both types of measurements can be made in all the regimes with either curved or flat surfaces. However, sinusoidal inputs must have a large enough amplitude if the existence of yield points are to be detected.

Friction Forces. Figure 14 shows three typical chart recorder friction traces for highly compressed PBD films of thickness $D \approx 10$ nm at three different sliding velocities: $V = 0.01$, 0.1, and 1.0 μm/s. The three curves show that the kinetic friction force $F_k = F$ is practically constant over a 2 order of magnitude change in the sliding velocity, V. In addition, the breaks in the curves, corresponding to the yield points, and the horizontal plateau regions corresponding to a constant friction force and to an effective viscosity given by eq 14 $\eta_{eff} \propto \dot{\gamma}^{-1}$, are indicative of pure frictional sliding.

Figure 15 shows the effect of velocity on the kinetic friction force F_k (as measured in the steady state plateau region) at different loads L. Being in the "hard-wall" regime of the forces, the film thicknesses remained almost constant at $D \approx 12$ nm. The range of velocities corresponds to shear rates of 10^2–10^3 s^{-1}. The results show that the friction force is independent of velocity at low loads, in accordance with Amontons' law, eq 4. Only at the highest load is there a noticeable increase or a maximum in F_k with V.

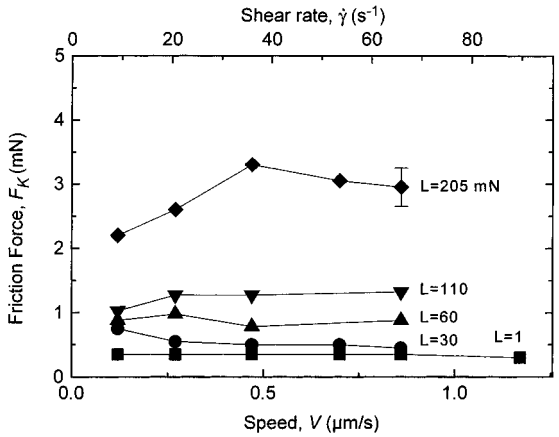

Figure 15. Effect of the shearing velocity V on the friction force F at different loads L.

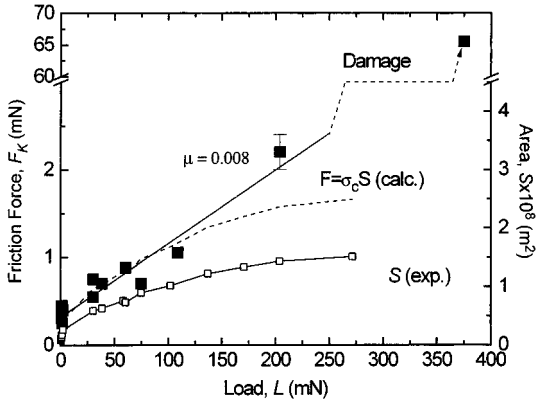

Figure 16. Frictional force F *vs* load L for polybutadiene films measured over a range of sliding speeds from 0.1 to 1.0 μm/s. The friction coefficient, defined by dF/dL is roughly constant at ~0.008, following Amontons' law, up to $L \approx 250$ mN. After that, damage is observed, and the friction force increases abruptly. The value of the critical shear stress is $\sigma_c = 1.1 \times 10^8$ Pa.

Similar measurements were made using both the bimorph slider drive and the friction device (motor) drive. The results were quantitatively the same over the same range of loads and sliding speeds.

The data of Figure 15 allow us to calculate the effective viscosity of the film using eq 14. This turns out to be very high (~10^4 Pa s). The same results are shown by the filled points in Figure 12A, where they are seen to extrapolate back to the rheological data, obtained during sinusoidal sliding at $L = 0$, along a line given by $\eta_{eff} \propto \dot{\gamma}^{-1}$. Also shown in Figure 12A are the shifts of the η_{eff} curves at different loads, L.

The measured friction force F was found to scale with the contact area, S, at low loads and with the load, L, at high loads (Figure 16). In addition, the contact area was well described by the JKR theory of "contact mechanics"[43] (Figure 16). These observations follow the theoretical expectations of the Bowden and Tabor model[44] as modified by Homola *et al.*[18] where the kinetic friction force is expected to obey the relation

$$F = C_1 S + C_2 L \tag{26}$$

where C_1 and $C_2 = \mu$ are constants. Fitting eq 26 to the results obtained for the PBD 7000 films (Figure 16) gave $C_1 = 1.1 \times 10^8$ Pa, and $C_2 = \mu = 0.008$. This low value for the "friction coefficient" μ is comparable to values obtained with some polymer melts such as perfluoropolyethers ($\mu = 0.024$).[45] We should note that

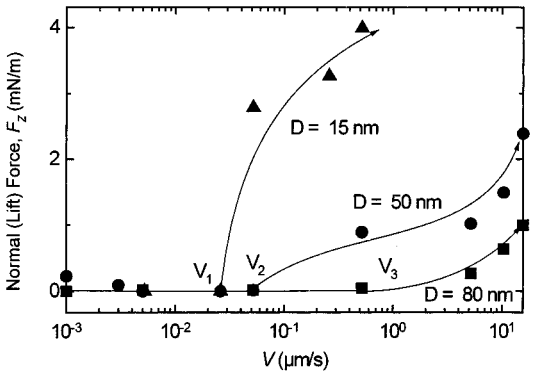

Figure 17. Normal force component F_z as a function of the shear velocity V at three different equilibrium film thicknesses.

film thickness did not change even at the highest applied loads where pressures as high as 14 MPa (140 atm) were reached, reaffirming the robustness of the last few polymer layers between the surfaces even under conditions of shear. However, once damage occurred to the mica surfaces, the friction coefficient increased dramatically to ~0.25—the value expected for damaged mica surfaces. This is consistent with previous observations on the friction of worn (damaged) mica surfaces in air or across various liquids.[46]

Normal Stress Component during Shear. We have observed a positive normal stress component in our shearing experiments, that is, upon shearing, the plates tend to separate unless they are prevented from doing this. This was observed most clearly when using weaker normal force-measuring springs (springs **S1** in Figures 2 and 3), which allowed any change in the normal component of the force between the surfaces to be measured during sliding. Typically, during the buildup to steady state sliding, the surfaces would separate from their initial, equilibrium separation and settle at some larger distance so long as shearing motion continued. The surfaces returned to their original separation soon (1 min) after the sliding was stopped. Figure 17 shows the value of this normal force F_z at three surface separations as a function of the maximum shear velocity (calculated from the driving amplitude and frequency). It is apparent that F_z has a critical onset velocity (V_1, V_2, and V_3 in Figure 17), above which it increases rapidly with V. The critical velocity is lower and the overall effect is more dramatic in thinner films.

This type of effect has been observed previously with polymer "brush" layers of zwitterion-terminated polystyrene end-grafted to mica in toluene.[36,47] These authors concluded that the phenomenon is due to a "coil-to-stretch" transition of the grafted coils on the surface, whereby the stretching decreases the screening of the segment—segment interactions within each brush layer, leading to an increased osmotic repulsion within the layers and between two opposing layers.[48]

In our system, the PBD is a pure homopolymer melt and therefore not expected to behave like an end-grafted brush layer in solution. However, the repulsive force profiles are similar to those obtained between brushes, and it has been suggested that the coils in contact with the surfaces remain effectively bound or "pinned" to the surfaces during the time scales of the interactions, even when these are very long. Thus, the interactions—both static and dynamic—of surfaces in polymer melts may not be too different from those of strongly end-adsorbed layers.

The observed effects may, however, be more general. It is well-known that polymer melts exhibit normal stresses upon shearing already in the bulk state.[1] Normal stresses result from the shear-induced alignment or orienting of previously entangled chains, and so can arise in both confined and bulk conditions. The bulk first normal stress difference σ_{z1} is proportional to $\dot{\gamma}^2$ at low shear rates and decreases its $\dot{\gamma}^2$-dependence at higher shear rates.[1] The behavior we observe in thin films is clearly different (see Figure 17) and so we conclude is a confinement effect. In fact, the similarity of our curves to the grafted polymer case[36] indicates that a similar mechanism might underlie both systems and that this may be a general effect in very thin polymer films.

Summary and Conclusions

We have studied the bulk and thin film behavior of polybutadiene and have analyzed the results using two different approaches: the rheological and tribological. Both static and dynamic measurements point towards nonbulk like, nonlinear behavior of PBD in films thinner than ~200 nm, the actual value depending on the measuring frequency or shear rate. The first nonbulk-like effect concerns an effectively immobilized surface layer of thickness comparable to R_g. This gives rise to a short-range monotonically repulsive force. However, the measured dynamic effects are much more complex than can be described by a simple shift in the position of the shear plane (cf. Figure 10). It is interesting to note that these findings are very similar to those previously reported by Israelachvili and Kott[26] for PBD films between surfaces vibrating in the normal plane, where the flow fields are expected to be quite different from those between two surfaces shearing laterally, as employed in the present study.

The second effect is a changed (increasing) viscosity of a sheared confined film, as previously reported by Hu and Granick.[8,9] The effective viscosity of PBD films was found to increase with increasing confinement and shear rate, and for 10 nm thick films it follows the relation $\eta_{eff} \propto \dot{\gamma}^n$, where for shear rates between 10^1 and 10^4 s^{-1} the exponent n is about -0.8 at low loads, increasing to about -1.0 with increasing load. We note that a value of -1.0 corresponds to the case of "ideal" friction, that is, to a friction force that is independent of the sliding velocity (Amontons' third law of friction).[49]

In this transition regime, the film is no longer bulk like, but is still describable by the WLF formalism, albeit with modified parameters from the bulk values. This should not be surprising: the WLF formalism is well suited to describing highly dissipative systems and so should be applicable to describing the dynamic properties of a thin film as it approaches the highly dissipative tribological regime. The applicability of the WLF formalism to friction has been demonstrated or discussed on a number of occasions[1,50,51] and recent friction force experiments[3,52,53] employing surfactant-coated mica surfaces at different loads, shearing velocities and temperatures have revealed the existence of bell-shaped $F(T)$ and $F(V)$ curves, obeying the time—temperature superposition principle, just as expected from the WLF theory.

In the case of confined complex fluids, such as polymer melts, a number of different relaxation processes may be occurring, some of which (for example, those involving chain-surface interactions) will have no bulk counterpart, while those that do may have significantly different relaxation times. A number of peaks and valleys may therefore be expected for such films.[53]

Further work, especially at different temperatures and over a larger range of frequencies, are needed to fully characterize the rheological behavior of confined liquids.

The third effect involves entry into the tribological regime where the concept of a shear viscosity no longer applies.[3,31,54,55] The tribological regime is characterized by yield points and discontinuous behavior that cannot be fitted into the WLF formalism, which implicitly assumes continuously changing variables, that is, that there are no abrupt phase transitions from one dynamic state to another as V or T changes.

It is interesting to compare our results with the very similar results recently obtained on a completely different system and using different experimental techniques. Thus, in their measurements of the forces and tribology of adsorbed poly-isoprene on cobalt surfaces interacting across a hydrocarbon solvent, Georges *et al.*[56] recently found the same nonlinear trends in the overall shapes of the normal force curves and friction traces, an increased friction at low shear rates, and similar relaxations when sliding is stopped. On the basis of these and other experiments, we have recently proposed a new formalism for relating friction forces to measurable parameters.[57]

Acknowledgment. This research was supported by the Department of Energy (DOE) under Grant DE-FG03-87ER45331 and by the Ministerio de Educación y Ciencia (Spain) under FPI Grant EX92-51359034.

References and Notes

(1) Ferry, J. D. *Viscoelastic Properties of Polymers*; Wiley: New York, 1980.
(2) Hatzikiriakos, S. G.; Dealy, J. M. *J. Rheol.* **1992**, *36*, 703.
(3) Yoshizawa, H.; Chen, Y.-L.; Israelachvili, J. *J. Phys. Chem.* **1993**, *97*, 4128.
(4) Montfort, J. P.; Tonck, A.; Loubet, J. L.; Georges, J. M. *J. Polym. Sci., Polym. Phys. Ed.* **1991**, *29*, 677.
(5) Israelachvili, J. N. In *Handbook of Micro/Nanotribology*; CRC Press, Inc.: Boca Raton, FL, 1995.
(6) Israelachvili, J. N.; Kott, S. J.; Fetters, L. J. *J. Polym. Sci., Polym. Phys. Ed.* **1989**, *27*, 489.
(7) Gee, M. L.; Israelachvili, J. N. *J. Chem. Soc., Faraday Trans.* **1990**, *86*, 4049.
(8) Hu, H.-W.; Carson, G. A.; Granick, S. *Phys. Rev. Lett.* **1991**, *66*, 2758.
(9) Granick, S. *Science* **1991**, *253*, 1347. Peachey, J.; Van Alsten, J.; Granick, S. *Rev. Sci. Instrum.* **1991**, *62*, 463.
(10) Hu, H.-W.; Granick, S. *Science* **1992**, *258*, 1339.
(11) Urbakh, M.; Daikhin, L.; Klafter, J. *Europhys. Lett.* **1995**, *32*, 125.
(12) Rabin, Y.; Hersht, I. *Physica A* **1993**, *200*, 708.
(13) Thompson, P. A.; Robbins, M. O.; Grest, G. S. *Isr. J. Chem.* **1995**, *35*, 93.
(14) Colby, R. H.; Fetters, L. J.; Graessley, W. W. *Macromolecules* **1987**, *20*, 2226. Our measured value of about 2.5 Pa s for the bulk shear viscosity of PBD 7000 is consistently lower than the value of 5 Pa s measured by Colby *et al.* We do not know the reason for this discrepancy, although aging effects in PBD samples are known to cause cross-linking and bring about significant changes in viscosity. Thus, for such samples, being above the entanglement molecular weight, the viscosity scales as $M^{3.4}$, so that a 23% difference or change in M could explain this discrepancy, which is entirely possible, since our polymer came from a different batch from that used by Colby *et al.* Other possible reasons for the discrepancy are discussed in the text.
(15) Israelachvili, J. N.; McGuiggan, P. M. *J. Mater. Res.* **1990**, *5*, 2223.
(16) Israelachvili, J. N. *Proc. R. Soc. London, A* **1972**, *A331*, 19.
(17) Tabor, D.; Winterton, R. *Proc. R. Soc. London, A* **1969**, *312*, 435.
(18) Homola, A. M.; Israelachvili, J. N.; Gee, M. L.; McGuiggan, P. M. *J. Tribol.* **1989**, *111*, 675.
(19) Israelachvili, J. N. *J. Colloid Interface Sci.* **1986**, *110*, 263.
(20) O'Neill, M. E. *Mathematica* **1964**, *11*, 67.
(21) O'Neill, M. E.; Stewartson, K. *J. Fluid Mech.* **1967**, *27*, 705.
(22) Goldman, A. J.; Cox, R. G.; Brenner, H. *Chem. Eng. Sci.* **1967**, *22*, 637.
(23) Chan, D. Y. C.; Horn, R. G. *J. Chem. Phys.* **1985**, *83*, 5311.
(24) Gee, M. L.; McGuiggan, P. M.; Israelachvili, J. N.; Homola, A. M. *J. Chem. Phys.* **1990**, *93*, 1895.
(25) Ferry[1] defines *linear* in a number of ways (cf. pp 2 and 11). Our criterion for linearity was that the response is directly proportional to the input, that it depends only on the frequency but not on the amplitude of deformation, and that a sinusoidal input produced a sinusoidal or nearly sinusoidal response. Depending on the film properties and system geometry, the response may be linear even for large strains (>1) as was found to be the case here for the thicker films undergoing lateral shear (Figure 8A).
(26) Israelachvili, J. N.; Kott, S. J. *J. Chem. Phys.* **1988**, *88*, 7162.
(27) Scheutjens, J. M. H. M.; Fleer, G. J. *Macromolecules* **1985**, *18*, 1882.
(28) Horn, R. G.; Hirz, S. J.; Hadziioannou, G.; Frank, C. W.; Catala, J. M. *J. Chem. Phys.* **1990**, *90*, 6767.
(29) Strictly, the restricted equilibrium repulsion may also be considered to arise from a finite viscosity effect, but one having a different origin and a much longer relaxation time.
(30) de Gennes, P.-G. *C. R. Acad. Sci. Paris, Ser 2* **1987**, *305*, 1181.
(31) Granick, S.; Hu, H.-W. *Langmuir* **1994**, *10*, 3857.
(32) Wang, Y.; Hill, K.; Harris, J. G. *Langmuir* **1993**, *9*, 1983.
(33) Horn, R. G.; Israelachvili, J. N. *Macromolecules* **1988**, *21*, 2836.
(34) Homola, A. M. *J. Chem. Phys.* **1991**, *94*, 2346.
(35) Montfort, J. P.; Hadziioannou, G. *J. Chem. Phys.* **1988**, *88*, 7187.
(36) Klein, J. *Pure Appl. Chem.* **1992**, *64*, 1577.
(37) Yoshizawa, H.; Israelachvili, J. N. *J. Phys. Chem.* **1993**, *97*, 11300.
(38) Ajdari, A; Brochard-Wyart, F; de Gennes, P-G; Leibler, L; Viovy, J-L; Rubinstein, M. *Physica A* **1994**, *204*, 17.
(39) Klein, J.; Kamiyama, Y.; Yoshizawa, H.; Israelachvili, J.; Fredrickson, G. H.; Pincus, P.; Fetters, L. J. *Macromolecules* **1993**, *26*, 5552.
(40) Johner, A.; Joanny, J. F. *J. Chem. Phys.* **1993**, *98*, 1647.
(41) Pelletier, E.; Montfort, J. P.; Loubet, J. L.; Tonck, A.; Georges, J. M. *Macromolecules* **1995**, *28*, 1990.
(42) Carson, G.; Hu, H.-W.; Granick, S. *Tribol. Trans.* **1992**, *35*, 405.
(43) Johnson, K. L.; Kendall, K.; Roberts, A. D. *Proc. R. Soc. London, A* **1971**, *324*, 301.
(44) Bowden, F. P.; Tabor, D. *Friction and Lubrication*; 2nd ed.; Methuen: London, 1967.
(45) Hirz, S. J.; Homola, A. M.; Hadziioannou, G.; Frank, C. *Langmuir* **1992**, *8*, 328.
(46) Homola, A. M.; Israelachvili, J. N.; McGuiggan, P. M.; Gee, M. L. *Wear* **1990**, *136*, 65.
(47) Klein, J.; Kumacheva, E.; Perahia, D.; Mahalu, D.; Warburg, S. *Faraday Discuss.* **1994**, *98*, 173.
(48) Rabin, Y.; Alexander, S. *Europhys. Lett.* **1990**, *13*, 49.
(49) The first law states that F is independent of the contact area; the second law states that it is proportional to the load.
(50) Grosch, K. A. *Nature* **1963**, *197*, 858.
(51) McLaren, K. G.; Tabor, D. *Nature* **1963**, *197*, 856.
(52) Liu, Y.; Wu, T.; Evans, D. F. *Langmuir* **1994**, *10*, 2241.
(53) Schmitt, F.-J.; Yoshizawa, H.; Schmidt, A.; Duda, G.; Knoll, W.; Wegner, G.; Israelachvili, J. *Macromolecules* **1995**, *28*, 3401.
(54) Israelachvili, J.; Chen, Y.-L.; Yoshizawa, H. *J. Adhesion Sci. Technol.* **1994**, *8*, 1.
(55) Reiter, G.; Levent Demirel, A.; Granick, S. *Science* **1994**, *263*, 1741.
(56) Georges, J-M.; Tonck, A.; Loubet, J-L.; Mazuyer, D.; Georges, E.; Sidoroff, F. *J. Phys. 2* (*Fr.*) **1996**, *6*, 57.
(57) Luengo, G.; Israelachvili, J.; Granick, S. *Wear* **1996**, *200*, 328.

MA9519122